IEEE Access
Multidisciplinary | Rapid Review | Open Access Journal

Received July 3, 2020, accepted July 8, 2020, date of publication July 13, 2020, date of current version July 24, 2020.

Digital Object Identifier 10.1109/ACCESS.2020.3008971

Robust Control for Unmanned Aerial Manipulator Under Disturbances

YANJIE CHEN[1,3], WEIWEI ZHAN[1], BINGWEI HE[1], LIXIONG LIN[1], ZHIQIANG MIAO[2,3], (Member, IEEE), XIAOFANG YUAN[2,3], AND YAONAN WANG[2,3]

[1]School of Mechanical Engineering and Automation, Fuzhou University, Fuzhou 350108, China
[2]College of Electrical and Information Engineering, Hunan University, Changsha 410082, China
[3]National Engineering Laboratory for Robot Visual Perception and Control Technology, Changsha 410082, China

Corresponding author: Weiwei Zhan (644074658@qq.com)

This work was supported in part by the National Key Research and Development Program of China under Grant 2018YFB1308200, in part by the National Natural Science Foundation of China under Project 61803089 and Project 61903135, in part by the Natural Science Foundation of Fujian Province under Grant 2019J01213, and in part by the Natural Science Foundation of Hunan Province under Grant 2020JJ5090.

ABSTRACT Unmanned aerial manipulator (UAM) is usually a combination of a quadrotor and a robotic arm that can exert active influences on the environments. The control problems of the UAM system include model uncertainty caused by its center of gravity shift and external disturbances from the environments. To handle these two disturbances, a tracking control strategy is proposed for position and attitude control of the UAM in this paper. In particular, the model of the UAM is established considering with center of gravity shift and disturbances from environments. In the position control, both internal disturbances and external disturbances are compensated by using a sliding mode controller. In the attitude control, an adaptive law is designed to estimate internal disturbances, and a disturbance observer is designed to estimate external disturbances. The stability analysis of the proposed controller is provided and the effectiveness of the proposed method is verified in simulation.

INDEX TERMS Adaptive control, center of gravity shift, disturbance observer, sliding mode control, unmanned aerial manipulator.

I. INTRODUCTION

Unmanned aerial robot systems have been substantially attracted researchers' attention all over the world due to their hovering and aggressive maneuvering ability [1]. Previous researches usually focus on monitoring and surveillance applications of unmanned aerial robots, which are limited to "look" and "search". However, the trend is changing that people are expected to utilize unmanned aerial robot systems with advanced manipulation capabilities for autonomous industrial maintenance and transportation tasks based on their superior mobility. The research sponsors also provide some projects aiming to develop UAV systems with manipulation capabilities, such as ARCAS, AEROARMS, and AEROWORKS [2]. Until recently, the unmanned aerial manipulator (UAM) has been applied in many different fields, such as agriculture, military, rescue, etc [3]–[6]. For example, Hoseong Seo *et al.* proposed vision-based guidance for the UAM to grasp a cylindrical object by using a stochastic model predictive approach [7]. Zhang *et al.* presented an independent control strategy for an aerial manipulator system composed of a hex-rotor and a 7-DOF manipulator to grasp a moving target [8]. R. Spica *et al.* studied the problem of trajectory planning that connected two arbitrary states while allowing the UAV to grasp a moving target at some intermediate time [9]. A. E. Jimenez-Cano *et al.* presented a quadrotor with a new kind of arm for assembly tasks [10]. Besides the above applications, the UAM has great potentials in extreme and harsh working conditions, such as cargo handling among the Antarctic research ships and scientific equipment recovery in dangerous environments.

Generally, manipulations of the UAM should overcome disturbances from the internal states' changes and external environments. In particular, the center of gravity (CoG) is different from its modeling value when the robotic arm moves or grasps objects. This error can be regarded as an internal disturbance, which has been investigated by much previous research. For example, a sliding battery box was designed to compensate for the center of gravity shift in a short time by adjusting the position of the mobile battery box [11]. A generalized gravity center estimation scheme was utilized to compensate for the center of gravity shift

The associate editor coordinating the review of this manuscript and approving it for publication was Shuping He.

[12]. The geometric parameters of the manipulator were optimized to minimize the center of gravity shift in [13]. Furthermore, the modeling errors including both system errors and environmental disturbances can be regarded as external disturbances. Similarly, some efforts had been attempted to improve the performance of the UAM under environmental disturbances. For example, a robust controller with a disturbance observer was designed to improve the position accuracy of the UAM in [14]. In [15], a controller based on a robust internal loop compensator (RIC) was proposed to achieve system stability and trajectory tracking under the effects of picking and placing a payload. A disturbance-compensated robust H_∞ controller and nonlinear model predictive control were used to improve the tracking performance of the UAM as well in [16] and [17]. Reference [18] provided a resilient control method to overcome uncertain disturbances for an intelligent vehicle. Reference [19] investigated robust H_∞ control for linear systems with poly-topic uncertainties. Reference [20] studied finite-time positiveness and distributed control problems for a class of Lipschitz nonlinear multi-agent systems. Reference [21] addressed finite-time boundedness and stabilization problems for n-neuron uncertain positive Markovian jumping neural networks (MJNNs). Reference [22] investigated the finite-time asynchronous control problem for continuous-time positive hidden Markov jump systems (HMJSs) by using the Takagi-Sugeno fuzzy model method.

Further, with the estimated physical properties and external disturbances, an augmented adaptive controller is proposed so that the UAM can carry an unknown payload and track the desired trajectory [23]. However, the designed controller can only be used in a specific environment. To avoid this issue, complex environments should be considered in the advanced controller design. References [24] and [25] designed nonlinear observers to estimate the model uncertainties as lumped tern and external disturbances, where the model uncertainties were treated as internal disturbances. Although many previous studies have considered internal disturbances and external disturbances in different environments, there are still many details worth to be considered. For example, these disturbances affect attitude decoupling and may cause attitude oscillation. The stability of the controller should be ensured under disturbances.

In this paper, both the internal and external disturbances are taken into account in the position and attitude control of the UAM. These disturbances are handled in two parts. In the position controller, the uncertain terms are compensated by a robust term and controlled by a sliding mode controller. In the attitude controller, an adaptive controller with disturbance observer (DOB) is designed to estimate internal disturbance and observe external disturbance. Overall, the contributions of this paper are listed as follows:

1) Considering to internal and external disturbances, the position controller is designed to ensure the tracking performance of the UAM under both these disturbances. At first, an intermediate variable is introduced to represent the state quantity. Then, based on the sliding mode controller, the traditional symbolic function is replaced by a saturation function, and a robust term is adopted to ensure that the intermediate variable is smooth. In this way, the problem of position deviation caused by the internal and external disturbances can be solved.
2) Before designing the attitude controller, the reference attitude angular velocity is filtered to make attitude control smoother. An adaptive controller with disturbance observer (DOB) is proposed to handle unknown internal and external disturbances in the attitude. The adaptive law has a good performance on the slowly changing internal disturbances. The DOB can be applied to various complex environments. As a result, the accuracy of attitude control can be improved in different environments under disturbances.

The rest of this paper is organized as follows. Section II provides the preliminary knowledge of the unmanned aerial manipulator system, including system model, dynamics of the UAM, and analysis on $\boldsymbol{\Delta_a}$ and $\boldsymbol{\Delta_c}$. Section III proposes the controller design and stability analysis. Section IV shows simulation comparisons for illustrating the effectiveness of the proposed method. Finally, the conclusions and future work are given in Section V.

Notation: For an n-dimensional vector $\boldsymbol{d_*} = [d_{*,1}, d_{*,2}, \cdots, d_{*,j}]$, $d_{*,j}(j = 1, 2, \cdots, n)$ represents the j^{th} element of $\boldsymbol{d_*}$. The symbol $\|\cdot\|$ is used to represent the Euclidean norm or its induced norm, which is defined as $\|\boldsymbol{d_*}\| = \sqrt{\boldsymbol{d_*^{\mathrm{T}} d_*}}$.

II. PRELIMINARIES

The UAM consists of two robot sub-systems, namely, a quadrotor and a multi-joint manipulator. Based on the model of the UAV, the model of the UAM is considered as a combination of the UAV and a robotic arm. In this section, the system modeling of the UAM is provided and equations of motion can be found in [26], [27] in Section II-A. Then, considering environmental disturbances and internal disturbances, the dynamic model of the UAM is derived in Section II-B. Furthermore, a detailed analysis of the internal disturbances and environmental disturbances follows in Section II-C.

A. SYSTEM MODEL

The coordinates of the UAM are established by the inertial frame $O_{\mathrm{W}} = \{X_{\mathrm{W}}, Y_{\mathrm{W}}, Z_{\mathrm{W}}\}$ and the quadrotor body-fixed frame $O_{\mathrm{B}} = \{X_{\mathrm{B}}, Y_{\mathrm{B}}, Z_{\mathrm{B}}\}$, respectively. The position of the UAM in the inertial frame represents the position of the body's center of mass. The position and attitude in the inertial frame O_{W} are represented by $\boldsymbol{X} = [x, y, z]^{\mathrm{T}}$ and $\boldsymbol{\Phi} = [\phi, \theta, \psi]^{\mathrm{T}}$, respectively, where the rotational associated coordinate $\boldsymbol{\Phi}$ is defined by the Euler angles (roll, pitch, and yaw). The control state of the UAM is defined as $\boldsymbol{q} = [\boldsymbol{X}; \boldsymbol{\Phi}]^{\mathrm{T}}$. Since the UAM is influenced by environmental disturbances, such as irregular wind and external force from the grasped

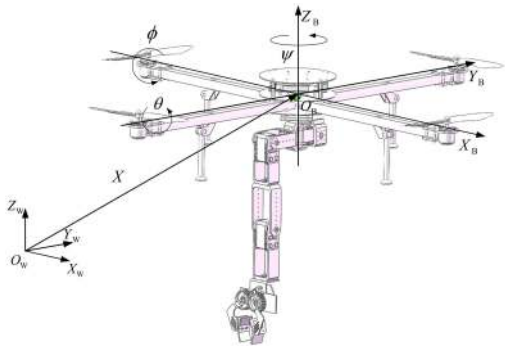

FIGURE 1. System model of the UAM.

object, the system model of the UAM can be written as

$$M(\boldsymbol{q})\ddot{\boldsymbol{q}} + C(\boldsymbol{q}, \dot{\boldsymbol{q}})\dot{\boldsymbol{q}} + G(\boldsymbol{q}) = \boldsymbol{f_m} + \boldsymbol{f_h}, \tag{1}$$

where $\ddot{\boldsymbol{q}}$, $\dot{\boldsymbol{q}}$, and $\boldsymbol{q}$ denote the acceleration, velocity, and position of the control states respectively. M represents the inertia matrix, C represents the Coriolis-centrifugal matrix. $\boldsymbol{f_m} = [f_{st}; \boldsymbol{f_{sa}}]^{\mathrm{T}}$ is the control input force vector, where f_{st} is the thruster force, and $\boldsymbol{f_{sa}} = [u_\phi, u_\theta, u_\psi]^{\mathrm{T}}$ is the attitude control torque. $\boldsymbol{f_h} = [\boldsymbol{f_{dt}}, \boldsymbol{f_{da}}]^{\mathrm{T}}$ is the external disturbance from environments, where $\boldsymbol{f_{da}} = [f_{da,1}, f_{da,2}, f_{da,3}]^{\mathrm{T}}$ is the influence of the external disturbance on the attitude of the UAM, and $\boldsymbol{f_{dt}}$ is the influence of the external disturbance on the position of the UAM.

B. DYNAMICS OF THE UAM

Using the Euler-Newton formula, the dynamics of the UAM system is expressed by the following equations [13], [28]:

$$m\ddot{X} + mS(\dot{\boldsymbol{\Omega}})X' + 2mS(\boldsymbol{\Omega})\dot{X}' + \boldsymbol{f_{dt}} + mS(\boldsymbol{\Omega})S(\boldsymbol{\Omega})X' = -f_{st}R(\boldsymbol{\Phi})\mathcal{I}_3 + mg\mathcal{I}_3, \tag{2}$$

$$J\dot{\boldsymbol{\Omega}} + S(\dot{X}')B + S(X')\dot{B} + S(S(\boldsymbol{\Omega})X')B + S(X')S(\boldsymbol{\Omega})B = \boldsymbol{f_{sa}} - S(\boldsymbol{\Omega})J\boldsymbol{\Omega} + \boldsymbol{f_{da}}, \tag{3}$$

where m denotes the total system mass, g is the gravitational acceleration, X' is the center of gravity position in the inertial frame O_{W}. $\boldsymbol{\Omega} = [p, q, r]^{\mathrm{T}}$ represents the angular velocity of the vehicle in body frame O_{B}. The impetus B is used to obtain the principle of conversation of angular momentum through the Newton equation, J is the inertia matrix in O_{B}, $S(\dot{\boldsymbol{\Omega}})$ represents the skew-symmetric operator associated with the cross product $\times$, $R(\boldsymbol{\Phi})$ is the rotational matrix representing the vehicle's body frame O_{B} to O_{W}. The angular velocity vector $\boldsymbol{\Omega}$ can be written with respect to $\boldsymbol{\Phi}$ as

$$\dot{\boldsymbol{\Phi}} = \mathcal{A}(\boldsymbol{\Phi})\boldsymbol{\Omega}, \tag{4}$$

where $\mathcal{A}(\boldsymbol{\Phi})$ is the translation matrix.

Assumption 1: The inertial tensor J is a constant matrix that does not be affected by changes in system geometry. Without loss of generality, it is assumed that J is diagonal because most bare quadrotors are shaped symmetrically in $\{X_{\mathrm{B}}, Y_{\mathrm{B}}, Z_{\mathrm{B}}\}$ directions.

Then, the J can be expressed as

$$J = \begin{bmatrix} I_x & & \\ & I_y & \\ & & I_z \end{bmatrix}. \tag{5}$$

The translational dynamics Eq.2 can be rewritten as

$$\ddot{X} + g\mathcal{I}_3 = \boldsymbol{G_x}\boldsymbol{\Theta} + \boldsymbol{\Delta_a} + \boldsymbol{f_{dt}}, \tag{6}$$

$$\boldsymbol{G_x} = \frac{f_{st}}{m}\boldsymbol{\Psi}, \boldsymbol{\Psi} = \begin{bmatrix} \mathrm{c}\psi & \mathrm{s}\psi & 0 \\ \mathrm{s}\psi & -\mathrm{c}\psi & 0 \\ 0 & 0 & \mathrm{c}\psi \end{bmatrix}, \boldsymbol{\Theta} = \begin{bmatrix} \mathrm{c}\phi\mathrm{s}\theta \\ \mathrm{s}\phi \\ \mathrm{c}\theta \end{bmatrix}, \tag{7}$$

where $\boldsymbol{\Delta_a}$ is the internal disturbance on the position, $\mathrm{c}\psi$ is the symbol of $\cos\psi$, $\mathrm{s}\psi$ is the symbol of $\sin\psi$.

The attitude translational dynamics Eq.3 can be rewritten as

$$I_x\dot{p} = u_\phi + (I_y - I_z)qr - m\Delta_{c,1}, \tag{8}$$

$$I_y\dot{q} = u_\theta + (I_z - I_x)pr - m\Delta_{c,2}, \tag{9}$$

$$I_z\dot{r} = u_\psi + (I_x - I_y)pq - m\Delta_{c,3}, \tag{10}$$

where p is the roll angular velocity, q is the pitch angular velocity, r is the yaw angular velocity, $\boldsymbol{\Delta_c} = [\Delta_{c,1}, \Delta_{c,2}, \Delta_{c,3}]^{\mathrm{T}}$ is the internal disturbance influence on the attitude.

C. ANALYSIS ON Δ_A AND Δ_C

Generally, two situations may make the UAM center of gravity shift. First, when a quadrotor is equipped with a robotic arm, the center of gravity of the new system does not coincide with the geometric center of the quadrotors. Especially when the robotic arm moves, this phenomenon becomes more serious. Second, when the UAM catches a target object, this non-coincidence phenomenon becomes particularly serious as well. The internal disturbances created by the center of gravity shift will affect the stability of the UAM.

According to [29], a widely used dynamic model of a simple quadrotor is shown as follows:

$$m\ddot{X} = -f_{st}R(\boldsymbol{\Phi})\mathcal{I}_3 + mg\mathcal{I}_3 - \boldsymbol{f_{dt}}, \tag{11}$$

$$J\dot{\boldsymbol{\Omega}} = \boldsymbol{f_{sa}} - S(\boldsymbol{\Omega})J\boldsymbol{\Omega} + \boldsymbol{f_{da}}. \tag{12}$$

Compared to the dynamics of the UAM in Eq.2 to Eq.3 and Eq.11 to Eq.12. It is observed that the difference can be expressed by the internal disturbance variables of the position and the attitude $\boldsymbol{\Delta_a}(\dot{X}, X', \boldsymbol{\Omega}, \dot{\boldsymbol{\Omega}})$ and $\boldsymbol{\Delta_c}(X, \ddot{X}', \dot{X}', \boldsymbol{\Omega})$, respectively. Since the internal disturbances are assumed as $\mathcal{C}^2$ and bounded, the $\boldsymbol{\Delta_a}$ and $\boldsymbol{\Delta_c}$ are accordingly included by $\mathcal{C}^2$ and bounded terms. Therefore, through dynamic analysis, the internal and external disturbances for the UAM are transferred to the position disturbance variable and attitude disturbance variable respectively. Consider the working conditions of the UAM, the $\boldsymbol{\Delta_a}$ and $\boldsymbol{\Delta_c}$ are the points that this paper is concerned on.

III. CONTROLLER DESIGN

In this section, a trajectory tracking controller of the UAM is designed. In the position controller, let $\boldsymbol{X_d} = [x_d, y_d, z_d]^{\mathrm{T}}$ be the reference trajectory, $\boldsymbol{X_d}$, $\dot{\boldsymbol{X}}_{\boldsymbol{d}}$ and $\ddot{\boldsymbol{X}}_{\boldsymbol{d}}$ are continuous and bounded. The position tracking error is defined as $\boldsymbol{\delta} = \boldsymbol{X} - \boldsymbol{X_d}$. The sliding mode function is defined as

$$\boldsymbol{s} = \dot{\boldsymbol{X}} - \dot{\boldsymbol{X}}_r, \tag{13}$$

where $\dot{\boldsymbol{X}}_r = \dot{\boldsymbol{X}}_d - \Lambda\boldsymbol{\delta}$, Λ is a diagonal gain matrix.

From Eq.13, the time derivative of $\boldsymbol{s}$ can be written as:

$$\dot{\boldsymbol{s}} = \ddot{\boldsymbol{X}} - \ddot{\boldsymbol{X}}_{\boldsymbol{d}} + \Lambda\dot{\boldsymbol{\delta}}. \tag{14}$$

Generally, the objective of position control for the UAM is to handle the control performances under the disturbances of $\boldsymbol{\Delta_1} = \boldsymbol{\Delta_a} + \boldsymbol{f_{dt}}$ [14]. The $\boldsymbol{\Delta_a}$ is the disturbance from the center of gravity shift. The $\boldsymbol{f_{dt}}$ is the disturbance from environmental factors, such as rain and wind. In the position controller, both these disturbances are handled together by introducing an intermediate variable $\boldsymbol{\eta}$. In particular, let $\eta_1 = \ddot{x} - \Delta_{1,1}$, $\eta_2 = \ddot{y} - \Delta_{1,2}$, and $\eta_3 = \ddot{z} - \Delta_{1,3}$, then $\boldsymbol{\eta} = [\eta_1, \eta_2, \eta_3]^{\mathrm{T}}$ is aimed to compensate the disturbances $\boldsymbol{\Delta_1} = [\Delta_{1,1}, \Delta_{1,2}, \Delta_{1,3}]^{\mathrm{T}}$ and ensures a good position tracking performance of the UAM.

Remark 1: In order to solve the problem of disturbances in position tracking, an intermediate variable $\boldsymbol{\eta}$ is used. The $\boldsymbol{\eta}$ is designed to compensate $\boldsymbol{\Delta_1} = [\Delta_{1,1}, \Delta_{1,2}, \Delta_{1,3}]^{\mathrm{T}}$ and then ensure the position tracking performance of $\boldsymbol{X}$. The relations between $\boldsymbol{\eta}$ and $\boldsymbol{X}$ are illustrated as follows:

$$\begin{cases} \dot{\boldsymbol{X}} = \boldsymbol{X_1}, \\ \dot{\boldsymbol{X}}_1 = \boldsymbol{\eta} + \boldsymbol{\Delta_1}. \end{cases} \tag{15}$$

Since the intermediate variable $\boldsymbol{\eta}$ is continuous and bounded, the intermediate variable is designed as follows:

$$\boldsymbol{\eta} = \ddot{\boldsymbol{X}}_d - \Lambda\dot{\boldsymbol{\delta}} - \beta\mathrm{sat}(\frac{\boldsymbol{s}}{\varepsilon/\rho_1}) - \frac{1}{\varepsilon}\rho_1^2\boldsymbol{s}, \tag{16}$$

where the saturation function can be described as:

$$\mathrm{sat}(\frac{\boldsymbol{s}}{\varepsilon/\rho_1}) = \begin{cases} \frac{|\,\boldsymbol{s}\,|}{\boldsymbol{s}}, & |\,\boldsymbol{s}\,| > \frac{\varepsilon}{\rho_1}, \\ \boldsymbol{s}, & |\,\boldsymbol{s}\,| \leq \frac{\varepsilon}{\rho_1}, \end{cases} \tag{17}$$

where ε is the constant satisfying $0 < \varepsilon \ll 1$, ρ_1 and β are positive constants. By choosing small enough ε, the disturbance $\boldsymbol{\Delta_1}$ can be compensated more accurately.

Proof: The following Lyapunov candidate function is defined as $V_1 = \frac{1}{2}\boldsymbol{s}^{\mathrm{T}}\boldsymbol{s} \geq 0$. The time derivative of V_1 can be expressed as

$$\dot{V}_1 = \boldsymbol{s}^{\mathrm{T}}\dot{\boldsymbol{s}} = \boldsymbol{s}^{\mathrm{T}}(\boldsymbol{\eta} + \boldsymbol{\Delta_1} - \ddot{\boldsymbol{X}}_{\mathrm{d}} + \Lambda\dot{\boldsymbol{\delta}}). \tag{18}$$

Substituting Eq.16 into Eq.18, the Eq.18 is rewritten as

$$\dot{V}_1 = \boldsymbol{s}^{\mathrm{T}}\boldsymbol{\Delta_1} - \beta\mathrm{sat}(\frac{\boldsymbol{s}}{\varepsilon/\rho_1})\boldsymbol{s}^{\mathrm{T}} - \frac{1}{\varepsilon}\rho_1^2\boldsymbol{s}^{\mathrm{T}}\boldsymbol{s}, \tag{19}$$

where $\boldsymbol{\Delta_1}$ is bounded as $\|\boldsymbol{\Delta_1}\| \leq \rho_1$.

Applying Young's inequality, i.e., $\boldsymbol{s}^{\mathrm{T}}\boldsymbol{\Delta_1} \leq \| \boldsymbol{s} \| \| \boldsymbol{\Delta_1} \| \leq \| \boldsymbol{s} \| \rho_1 \|$ for two vectors $\boldsymbol{s}$ and $\boldsymbol{\Delta_1}$, then Eq.19 yields

$$\dot{V}_1 \leq \| \boldsymbol{s} \| \| \boldsymbol{\Delta_1} \| - \beta\mathrm{sat}(\frac{\boldsymbol{s}}{\varepsilon/\rho_1})\boldsymbol{s}^{\mathrm{T}} - \frac{1}{\varepsilon}\rho_1^2\boldsymbol{s}^{\mathrm{T}}\boldsymbol{s}. \tag{20}$$

When $\| \boldsymbol{s} \| \rho_1 > \varepsilon$, the time derivative of V_1 is rewritten as

$$\dot{V}_1 \leq -\beta \| \boldsymbol{s} \| + (1 - \frac{1}{\varepsilon} \| \boldsymbol{s} \| \rho_1) \| \boldsymbol{s} \| \rho_1 < 0. \tag{21}$$

When $\| \boldsymbol{s} \| \rho_1 \leq \varepsilon$, the time derivative of V_1 can be rewritten as

$$\dot{V}_1 \leq -\frac{\beta}{\varepsilon/\rho_1}\boldsymbol{s}^{\mathrm{T}}\boldsymbol{s} + \varepsilon \leq -\frac{2\beta}{\varepsilon/\rho_1}V_1 + \varepsilon, \tag{22}$$

$$0 \leq V_1 \leq \frac{\varepsilon^2}{2\beta\rho_1} + (V_1(0) - \frac{\varepsilon^2}{2\beta\rho_1})\exp^{-2\beta\rho_1 t/\varepsilon}, \quad \forall t \geq 0, \tag{23}$$

As a result, the sliding mode surface satisfies $\|s(t)\| \leq \sqrt{\varepsilon^2/\beta\rho_1}$. By increasing β and ρ_1 or decreasing ε, the upper bound $\sqrt{\varepsilon^2/\beta\rho_1}$ can be made arbitrarily small [23]. Consequently, $\boldsymbol{s}$ can be made arbitrarily small. Thus, finite-time convergence and the boundedness of s can be achieved simultaneously. The proof is complete.

With the designed intermediate variable $\boldsymbol{\eta}$, a corrected attitude reference $\boldsymbol{\Phi_r} = [\phi_r, \theta_r, \psi_r]^{\mathrm{T}}$ that can compensate $\boldsymbol{\Delta_1}$ is calculated from Eq.6 in following formula

$$\boldsymbol{\Theta_r} = \boldsymbol{G_x}^{-1}(\boldsymbol{\eta} + g\mathcal{I}_3) \tag{24}$$

Then the thruster force f_{st} can be rewritten as

$$f_{st} = m(\boldsymbol{\eta} + g\mathcal{I}_3)\boldsymbol{\Psi}^{-1}\boldsymbol{\Theta_r}^{-1} \tag{25}$$

The attitude of the UAM includes roll, pitch, and yaw. Taking the roll angle as an example, the design of the attitude controller is explained. Pitch angle and yaw angle are given similar control laws. An adaptive controller with disturbance observer (DOB) is designed for the attitude controller. In particular, the adaptive estimator is designed to approximate the internal disturbance $\boldsymbol{\Delta_c}$. The DOB is designed to observe external disturbance $\boldsymbol{f_{da}}$.

Define the angle error $e_1 = \phi - \phi_r$, and then its derivative is

$$\dot{e}_1 = p - \dot{\phi}_r. \tag{26}$$

Define the angular velocity error $\chi_1 = p - p_r$. Designing a virtual control law for p_r, the virtual control vector p_{rf} is

$$p_{rf} = v_1 + \dot{\phi}_r, \tag{27}$$

where v_1 is the robust control term that needs to be designed.

Remark 2: After attitude decoupling, the attitude controller has to track a high-frequency reference trajectory in a short period of time. However, since the UAM is easily affected by the environment, it is expected to have a smooth trajectory. To handle this problem, the variable p_r is obtained by letting p_{rf} pass through a first-order filter with a constant α:

$$\alpha\dot{p}_r + p_r = p_{rf}, p_r(0) = p_{rf}(0), \tag{28}$$

where the time constant α satisfies $0 < \alpha \ll 1$. Here, a first-order filter is used to compute p_r from p_{rf}, because if p_{rf} is directly used in control input, p_{rf} may cause high-frequency oscillation [30].

Before proofing the stability of the proposed control law, χ_{1f} is described in more detail. Define a filtered error L as

$$L = p_r - p_{rf}. \tag{29}$$

First, note that

$$p - p_{rf} = p - p_r + p_r - p_{rf} = \chi_1 + L. \tag{30}$$

The filtered error $L \to 0$ if the time constant α is small enough. In the standard stability analysis of the dynamic surface control method, L is treated as a new state variable. Thus, a robust control term v_1 is needed to surpass it. Based on the preceding analysis, it can be obtained:

$$\begin{cases} \dot{e}_1 = v_1 + \chi_1 + L, \\ \dot{\chi}_1 = \dot{p} - \dot{p}_r. \end{cases} \tag{31}$$

The control law u_ϕ on the roll attitude for UAV is designed as the following equation:

$$u_\phi = -k_2\chi_1 - e_1 + (I_z - I_y)qr + m\hat{\Delta}_{c,1} + I_x\dot{p}_r - \hat{f}_{da,1}, \tag{32}$$

where $\hat{\Delta}_{c,1}$ represents the estimated internal disturbance, $\hat{f}_{da,1}$ represents the DOB of external disturbance.

Proof: Let us consider the following Lyapunov candidate function

$$V_2 = \frac{1}{2}I_x\chi_1^2 + \frac{1}{2}e_1^2 + \frac{1}{2\xi_1}\tilde{\Delta}_{c,1}^2, \tag{33}$$

where the estimated error of internal disturbance $\tilde{\Delta}_{c,1}$ is defined as $\tilde{\Delta}_{c,1} = \hat{\Delta}_{c,1} - \Delta_{c,1}$.

The time derivative of V_2 can be expressed as

$$\begin{aligned} \dot{V}_2 &= I_x\chi_1\dot{\chi}_1 + e_1\dot{e}_1 + \frac{1}{\xi_1}\tilde{\Delta}_{c,1}\dot{\tilde{\Delta}}_{c,1} \\ &= \chi_1(I_x\dot{p} - I_x\dot{p}_r) + e_1(v_1 + \chi_1 + L) + \frac{1}{\xi_1}\tilde{\Delta}_{c,1}\dot{\tilde{\Delta}}_{c,1}. \end{aligned} \tag{34}$$

Using the control law Eq.32, the time derivative of V_2 results in

$$\begin{aligned} \dot{V}_2 = &-k_2\chi_1^2 + \chi_1(f_{da,1} - \hat{f}_{da,1}) + e_1(v_1 + L) \\ &+ [m\chi_1 + \frac{1}{\xi_1}\dot{\tilde{\Delta}}_{c,1}]\tilde{\Delta}_{c,1}. \end{aligned} \tag{35}$$

Assuming that $\Delta_{c,1}$ changes very slowly compared with the adaptation rate for uncertainty $\hat{\Delta}_{c,1}$, the update rule for the estimated uncertainty $\hat{\Delta}_{c,1}$ can be written as

$$\dot{\hat{\Delta}}_{c,1} = -\xi_1 m\chi_1, \tag{36}$$

where ξ_1 is a positive constant.

The robust control term v_1 is designed as

$$v_1 = -k_1e_1 + \rho_L\mathrm{sgn}(e_1), \tag{37}$$

where ρ_L is a positive constant. Due to the bound on L depends on $\dot{p}_r$, the filtered error L is bounded as $|L| \le \rho_L$.

The DOB $\hat{f}_{da,1}$ is designed as

$$\hat{f}_{da,1} = \frac{\rho_a^2\chi_1}{\rho_a|\chi_1| + \nu_1}, \tag{38}$$

where ρ_a is a positive constant, ν_1 is an arbitrarily small positive constant. The external disturbance $\boldsymbol{f_{da}}$ is bounded as $\| \boldsymbol{f_{da}} \| \le \rho_a$.

From Eq.36, Eq.37, and Eq.38, the time derivative of the Lyapunov candidate function V_2 can be rewritten as

$$\begin{aligned} \dot{V}_2 &= -k_2\chi_1^2 + e_1(-k_1e_1 + \rho_L\mathrm{sgn}(e_1) + L) \\ &\quad + \chi_1(f_{da,1} - \frac{\rho_a^2\chi_1}{\rho_a|\chi_1| + \nu_1}) \\ &\le -k_2 \mid \chi_1 \mid^2 - k_1 \mid e_1 \mid^2 + \rho_L|e_1| - \rho_L|e_1| \\ &\quad - \frac{\rho_a^2\chi_1^2}{\rho_a|\chi_1| + \nu_1} + \rho_a|\chi_1| \\ &= -k_2 \mid \chi_1 \mid^2 - k_1 \mid e_1 \mid^2 + \frac{\rho_a|\chi_1|}{\rho_a|\chi_1| + \nu_1}\nu_1, \end{aligned} \tag{39}$$

Since $0 \le \rho_a|\chi_1| \le \rho_a|\chi_1| + \nu_1$, the time derivative of Lyapunov candidate function V_2 can be rewritten as

$$\dot{V}_2 \le -k_2 \mid \chi_1 \mid^2 - k_1|e_1|^2 + \nu_1. \tag{40}$$

At this point, the Lyapunov candidate function V_2 is reconsidered:

$$V_2 \le (\frac{I_x}{2} + \frac{1}{2})(|e_1|^2 + |\chi_1|^2) + \frac{\mid \xi^{-1} \mid}{2} \mid \tilde{\Delta}_{c,1} \mid^2 = \overline{V}_2. \tag{41}$$

From Eq.40, and Eq.41, the time derivative of V_2 is bounded as

$$\begin{aligned} \dot{V}_2 &\le -k_2 \mid \chi_1 \mid^2 - k_1 \mid e_1 \mid^2 + \nu_1 \\ &\le -\kappa_1\overline{V}_2 + \kappa_2 \mid \bar{\Delta}_{c,1} \mid^2 + \nu_1 \\ &\le -\kappa_1\overline{V}_2 + \gamma, \end{aligned} \tag{42}$$

where $\mid \tilde{\Delta}_{c,1} \mid^2 \le \bar{\Delta}$, $\kappa_1 = \kappa_3/(\frac{I_x}{2} + \frac{1}{2})$, $\kappa_3 = \min\{k_1, k_2\}$, $\kappa_2 = \frac{|\xi^{-1}|}{2}\kappa_1$, and $\gamma = \kappa_2\bar{\Delta} + \nu_1$.

If $\kappa_1 \ge \gamma/\rho_V$ with respect to positive constant ρ_V, then it is shown that $\dot{V}_2 \le 0$ with $V_2 = \rho_V$. When $V_2 \le \rho_V$, the inequality Eq.42 implies

$$0 \le V_2(t) \le \frac{\gamma}{\kappa_1} + (V_2(0) - \frac{\gamma}{\kappa_1})\exp^{-\kappa_1 t}, \quad \forall t \ge 0. \tag{43}$$

This proves that the design of the DOB and estimator can make $p_r \to p_{rf}$ and the angular velocity error χ_1 converge to zero in a limited time.

Lyapunov-like analysis proves that the proposed adaptive law can make the system stable asymptotically by using the Barbalat's lemma based on [31]. Correspondingly, the q_{rf}, r_{rf}, u_θ, and u_ψ can be respectively designed as

$$q_{rf} = -k_3e_2 + \rho_L\mathrm{sgn}(e_2) + \dot{\theta}_r, \tag{44}$$

$$r_{rf} = -k_5e_3 + \rho_L\mathrm{sgn}(e_3) + \dot{\psi}_r, \tag{45}$$

TABLE 1. D-H parameters of the active manipulator.

j	α_{j-1}(rad)	a_{j-1}(m)	d_j(m)	θ_j(rad)
1	0	0.03	0	θ_1
2	$-\frac{\pi}{2}$	0.06	0	θ_2
3	0	0.08	0	θ_3
4	0	0.03	0	0

$$u_\theta = -k_4\chi_2 - e_2 + (I_x - I_z)pr - \int_0^t \xi_2 m^2 \chi_2 \mathrm{d}t + \dot{q}_r + \frac{\rho_a^2 \chi_2}{\rho_a|\chi_2| + \nu_2}, \tag{46}$$

$$u_\psi = -k_6\chi_3 - e_3 + (I_y - I_x)pq - \int_0^t \xi_3 m^2 \chi_3 \mathrm{d}t + \dot{r}_r + \frac{\rho_a^2 \chi_3}{\rho_a|\chi_3| + \nu_3}, \tag{47}$$

where $e_2 = \theta - \theta_r$ is the error of the pitch angle, $e_3 = \psi - \psi_r$ is the error of the yaw angle, $\chi_2 = q - q_r$ is the error of the pitch angular velocity, $\chi_3 = r - r_r$ is the error of the yaw angular velocity, $k_i (i = 3, \cdots, 6)$, ν_i, $\xi_i (i = 2, 3)$ are positive constants. Computing q_r, r_r from $\alpha\dot{q}_r + q_r = q_{rf}$, $q_r(0) = q_{rf}(0)$, $\alpha\dot{r}_r + r_r = r_{rf}$, $r_r(0) = r_{rf}(0)$.

IV. SIMULATION VERIFICATION

The proposed control method is verified in MATLAB environments. In simulations, the UAM burdens internal disturbances generated by the robotic arm grasping the target and external disturbances from the environments. Then, two control methods are compared in this section. In particular, the performances of the proposed controller are evaluated by comparing the results of the controller in [23]. To verify the performance of this method, comparisons are conducted in two different scenarios in the attitude control. In the first scenario, the rate of change of external disturbances is zero, which means that $\dot{\boldsymbol{f}}_{da} = 0$. But the external environment changes at every moment. In the second scenario, the UAM suffers an external disturbance in the 30s, and the external disturbances are changing as well. For the controller of [23], the gains and update rates are the same as the proposed controller in two different scenarios. The RMSE criterion is used as a standard for control performance evaluation.

A. EXPERIMENTAL SETUP

The UAM weighs about 1.9 kg, including both a quadrotor body and a manipulator. The grasping target weighs 1 kg. The parameters of the position controller are set as follows: $\Lambda = \mathrm{diag}\{3, 3, 3\}$, $\beta = 1.5$, $\rho_1 = 0.6$, $\varepsilon = 0.1$. The parameters of the attitude controller are set as follows: $k_i = 6, (i = 1, \cdots, 6)$, $\xi_i = 0.02$, $\nu_i = 0.01, (i = 1, 2, 3)$, $\rho_L = 0.001$, $\rho_a = 0.4$. The time constant α is set as 0.01. The simulation duration is the 50s. The simulation step size is fixed as 0.01. The yaw angle is always zero throughout the simulations. The configurations of the manipulator are described by the Denavit-Hartenberg parameters with respect to O_B shown in Table 1.

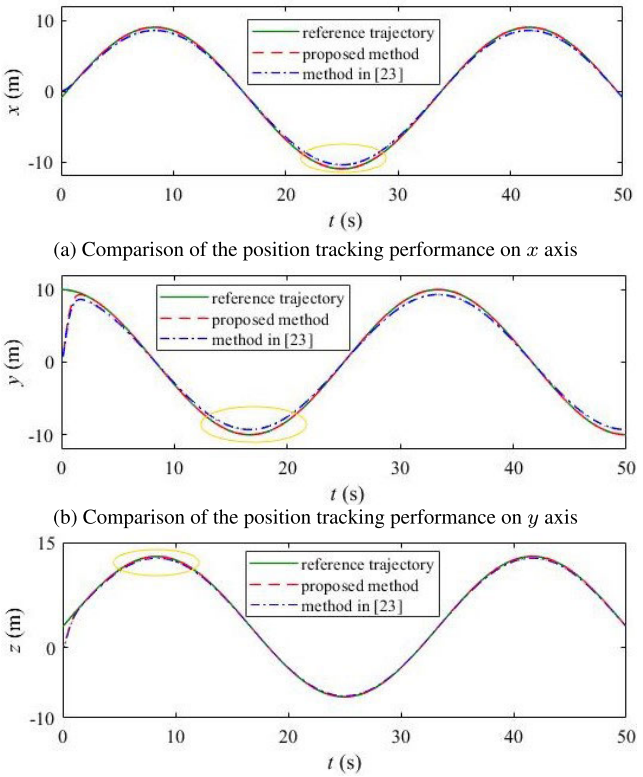

(a) Comparison of the position tracking performance on x axis

(b) Comparison of the position tracking performance on y axis

(c) Comparison of the position tracking performance on z axis

FIGURE 2. Position tracking performances by two controllers.

The disturbances of the robotic arm's joints are set as follows:

$$\begin{cases} \theta_1 = 0.01\pi t, \\ \theta_2 = 0.01\pi(25 - t), \\ \theta_3 = 0.01\pi(1.2t - 60), \\ 0 \le t \le 50. \end{cases} \tag{48}$$

B. RESULTS AND ANALYSIS

At first, suppose the UAM can perfectly maintain the desired attitude. The compared tracking performances of the position are shown in Fig.2. From Fig.2(a)-(c), the position tracking performances of both methods can track the reference trajectory within 8s. However, the position controller in [23] cannot follow the reference trajectory because of steady-state errors existing in three axes. It is because that there is no attitude decoupling, and $\boldsymbol{\Phi}_0$ is adopted by ignoring the disturbances $\boldsymbol{\Delta_1}$ instead of the corrected attitude reference (desired) $\boldsymbol{\Phi}_r$ in [23]. As a result, the steady-state errors become greater especially when the UAM moves away from the original point in x and y directions, which are labeled within a yellow circle in Fig.2.

In order to illustrate the performance clearly, the statistical data of both the proposed method and the compared method based on the Root Mean Squared Error (RMSE) criterion are provided in Table 2. From Table 2, the position tracking errors in three axes by the proposed controller are smaller than that by the compared control method.

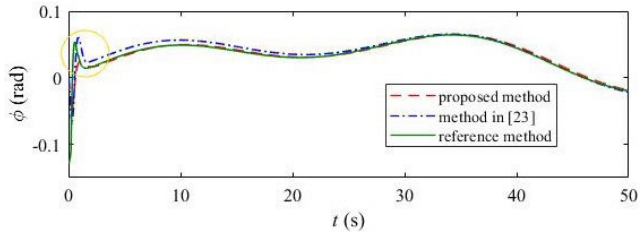

(a) Comparison of the angle ϕ tracking performance

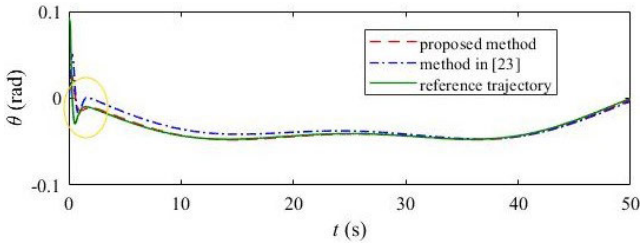

(b) Comparison of the angle θ tracking performance

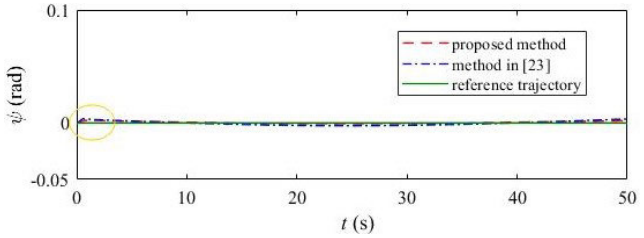

(c) Comparison of the angle ψ tracking performance

FIGURE 3. Attitude tracking performances by two controllers in the first scenario.

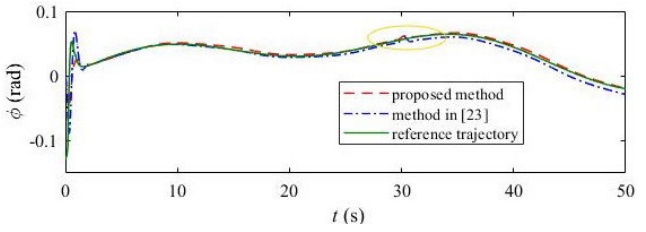

(a) Comparison of the angle ϕ tracking performance

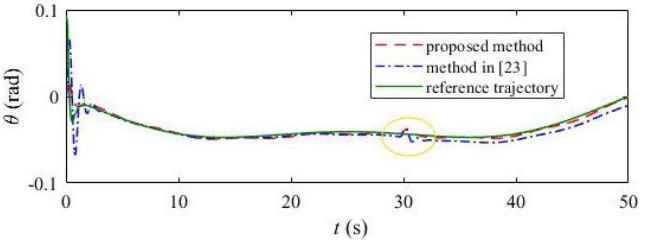

(b) Comparison of the angle θ tracking performance

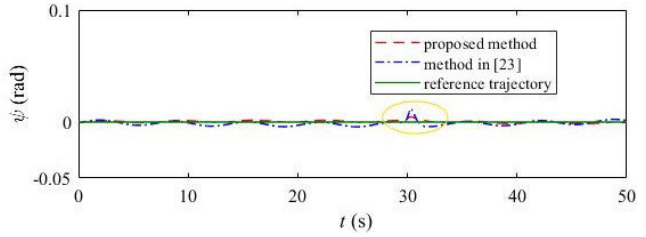

(c) Comparison of the angle ψ tracking performance

FIGURE 4. Attitude tracking performances by two controllers in the second scenario.

TABLE 2. Comparisons performance in the position control (RMSE).

	Proposed method	Method in [23]
x(m)	0.0485	0.1176
y(m)	0.5385	0.5712
z(m)	0.1676	0.1676

Second, in the attitude control, the reference attitude trajectory does not always start from zero. In the first scenario, the UAM is affected by a constant disturbance. The comparative tracking performances of attitudes between the proposed method and the controller in [23] are shown in Fig.3(a)-(c). In particular, from Fig.3(a)-(b), the overshoot of the reference trajectory in the first two seconds is much greater than the overshoot of the next two seconds. For a second-order system, a large amplitude oscillation will be generated when tracking this kind of reference trajectory. Meanwhile, the UAM is susceptible to environmental impact, it is expected to be able to smoothly follow the reference trajectory, which is conducive to the UAM resisting environmental disturbances and stable gripping of the robotic arm. From the yellow circles labeled in Fig.3(a)-(b), the first-order filter processing of the reference attitude trajectory can effectively reduce the UAM oscillation. Therefore, the attitude controller with adaptive law estimation of $\boldsymbol{\Delta_c}$ and the DOB of $\boldsymbol{f_{da}}$ can make the UAM perfectly follow reference trajectories in a limited time. As a result, the attitude controller of the proposed method can improve convergence speed and reduce overshoot by disturbances estimations.

Furthermore, the external environment is not always constant but changes. In the second scenario, the UAM is working on a rapidly changing environment. The attitude tracking performances of the proposed method and the controller in [23] are compared in Fig.4(a)-(c). From Fig.4(a)-(c), the proposed method can follow the reference trajectory with smaller steady-state error existence. In particular, the DOB of $\boldsymbol{f_{da}}$ can make the UAM more perfectly follow the reference trajectory in a limited time. As a result, all attitude trajectories by the proposed method follow their reference without noticeable biases. In particular, within the yellow circle regions shown in Fig.4(a)-(c), the DOB of the proposed method observes the $f_{da,1}$ with small error and is sensitive to the shock response. However, the estimator of [23] can not accurately estimate the $f_{da,1}$ which results in larger errors in the attitude control. To illustrate this phenomenon clearly, the estimator errors between two controllers in two scenarios are shown in Fig.5. From Fig.5(a), in the first scenario, the DOB of the proposed method observes the $f_{da,1}$ smoothly and accurately in 10s. In contrast, the method in [23] needs 20s to estimate the $f_{da,1}$. From Fig.5(b), in the second scenario, the proposed method can recover more efficiently compared to the controller in [23].

To illustrate the performance clearly, the compared results in two scenarios based on the Root Mean Squared Error (RMSE) criterion are provided in Table 3 and Table 4 respectively. From Table 3 and Table 4, whether the

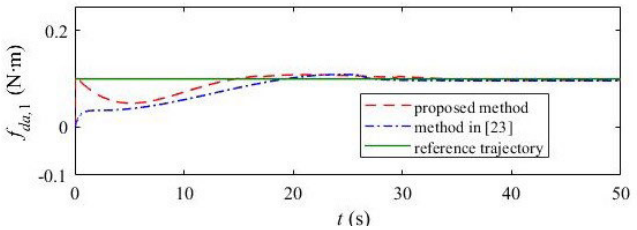

(a) Results of $f_{da,1}$ by two controllers in the first scenario

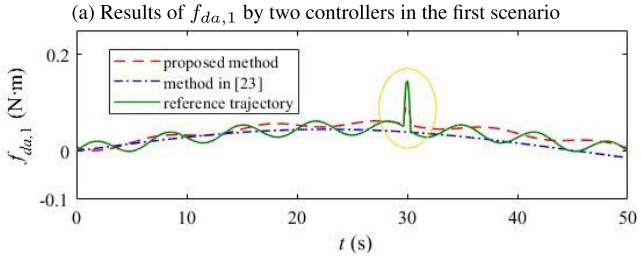

(b) Results of $f_{da,1}$ by two controllers in the second scenario

FIGURE 5. Results of $f_{da,1}$ by two controllers in two scenarios.

UAM is in scenarios with dynamic disturbances or static disturbances, the proposed method shows higher tracking accuracy and smoother tracking performance. In the first scenario, Table 3 shows that the tracking accuracy of the proposed method is slightly higher than the compared method. In the second scenario, Table 4 shows that the proposed method can allow the UAM to maintain high-precision trajectory tracking the same as that in the first scenario. However, the method in [23] makes the UAM severely affected in a dynamic scenario.

Overall, the trajectory tracking performance of the proposed method is more preferable when the UAM is working outdoors with unknown and nonlinear disturbances both from internal states' changes and external environmental influences.

TABLE 3. Comparisons performance in the attitude control in first scenario (RMSE).

	Proposed method	Method in [23]
ϕ(rad)	0.0422	0.0483
θ(rad)	0.0222	0.0286
ψ(rad)	6.1043×10^{-4}	0.0018

TABLE 4. Comparisons performance in the attitude control in second scenario (RMSE).

	Proposed method	Method in [23]
ϕ(rad)	0.0311	0.0513
θ(rad)	0.0224	0.0470
ψ(rad)	0.0012	0.0028

V. CONCLUSION

To handle the problems of the UAM system grasping objects under uncertain environmental disturbances, such as continuous rain and wind, a robust control strategy is proposed in this paper. At first, the disturbances are divided into two classes, namely, the internal disturbances from the center of gravity shift and external disturbances from environments. Then, in the position control, both internal and external disturbances are handled by a sliding mode controller. In the attitude control, the internal disturbances are estimated by an adaptive law and external disturbances are estimated by the DOB. Both disturbances estimations are embedded in a controller. Finally, the proposed method is compared with the controller without disturbances compensation in simulations. The results verify the effectiveness of the proposed method.

However, the model uncertainties include the total mass of the UAM after target grasping. For example, when the UAM grasps a sponge, the mass of the sponge may become heavier on a rainy day. It generates challenges of stable control for the UAM. Therefore, to ensure the safety of the UAM operation, this kind of uncertainty will be considered in future applications. In particular, a safety-enhanced mechanism for grasping or throwing away will be considered when the uncertainties reach the limitation of the UAM. An accurate online estimation method for the mass of the target will be designed to ensure the stable control of the UAM.

REFERENCES

[1] F. Ruggiero, V. Lippiello, and A. Ollero, "Aerial manipulation: A literature review," *IEEE Robot. Autom. Lett.*, vol. 3, no. 3, pp. 1957–1964, Jul. 2018.
[2] A. Santamaria-Navarro, P. Grosch, V. Lippiello, J. Solà, and J. Andrade-Cetto, "Uncalibrated visual servo for unmanned aerial manipulation," *IEEE/ASME Trans. Mechatronics*, vol. 22, no. 4, pp. 1610–1621, Aug. 2017.
[3] C. Liu, A. Bera, T. Tsabedze, D. Edgar, and M. Yim, "Spiral zipper manipulator for aerial grasping and manipulation," in *Proc. IEEE Int. Conf. Intell. Robots Syst. (IROS)*, Nov. 2019, pp. 3179–3184.
[4] D. Mellinger, Q. Lindsey, M. Shomin, and V. Kumar, "Design, modeling, estimation and control for aerial grasping and manipulation," in *Proc. IEEE Int. Conf. Intell. Robots Syst.*, Sep. 2011, pp. 2668–2673.
[5] G. Loianno, Y. Mulgaonkar, C. Brunner, D. Ahuja, A. Ramanandan, M. Chari, S. Diaz, and V. Kumar, "Smartphones power flying robots," in *Proc. IEEE Int. Conf. Intell. Robots Syst.*, Sep. 2015, pp. 1256–1263.
[6] P. E. I. Pounds and A. M. Dollar, "Stability of helicopters in compliant contact under PD-PID control," *IEEE Trans. Robot.*, vol. 30, no. 6, pp. 1472–1486, Dec. 2014.
[7] H. Seo, S. Kim, and H. J. Kim, "Aerial grasping of cylindrical object using visual servoing based on stochastic model predictive control," in *Proc. IEEE Int. Conf. Robot. Autom.*, May/Jun. 2017, pp. 6362–6368.
[8] G. Zhang, Y. He, B. Dai, F. Gu, L. Yang, J. Han, G. Liu, and J. Qi, "Grasp a moving target from the air: System & control of an aerial manipulator," in *Proc. IEEE Int. Conf. Robot. Autom.*, May 2018, pp. 1681–1687.
[9] R. Spica, A. Franchi, G. Oriolo, H. H. Bülthoff, and P. R. Giordano, "Aerial grasping of a moving target with a quadrotor UAV," in *Proc. IEEE Int. Conf. Intell. Robots Syst.*, Oct. 2012, pp. 4985–4992.
[10] A. E. Jimenez-Cano, J. Martin, G. Heredia, A. Ollero, and R. Cano, "Control of an aerial robot with multi-link arm for assembly tasks," in *Proc. IEEE Int. Conf. Robot. Autom.*, May 2013, pp. 4916–4921.
[11] F. Ruggiero, M. A. Trujillo, R. Cano, H. Ascorbe, A. Viguria, C. Peréz, V. Lippiello, A. Ollero, and B. Siciliano, "A multilayer control for multirotor UAVs equipped with a servo robot arm," in *Proc. IEEE Int. Conf. Robot. Autom.*, May 2015, pp. 4014–4020.
[12] E. Fresk, D. Wuthier, and G. Nikolakopoulos, "Generalized center of gravity compensation for multirotors with application to aerial manipulation," in *Proc. IEEE Int. Conf. Intell. Robots Syst.*, Sep. 2017, pp. 4424–4429.
[13] M. Kamel, K. Alexis, and R. Siegwart, "Design and modeling of dexterous aerial manipulator," in *Proc. IEEE Int. Conf. Intell. Robots Syst.*, Oct. 2016, pp. 4870–4876.
[14] S. Kim, S. Choi, H. Kim, J. Shin, H. Shim, and H. J. Kim, "Robust control of an equipment-added multirotor using disturbance observer," *IEEE Trans. Control Syst. Technol.*, vol. 26, no. 4, pp. 1524–1531, Jul. 2018.
[15] A. Khalifa, M. Fanni, A. Ramadan, and A. Abo-Ismail, "Controller design of a new quadrotor manipulation system based on robust internal-loop compensator," in *Proc. IEEE Int. Conf. Auto. Robot Syst. Competitions*, Apr. 2015, pp. 97–102.
[16] G. Garimella and M. Kobilarov, "Towards model-predictive control for aerial pick-and-place," in *Proc. IEEE Int. Conf. Robot. Autom.*, May 2015, pp. 4692–4697.

[17] K. Lee, J. Back, and I. Choy, "Nonlinear disturbance observer based robust attitude tracking controller for quadrotor UAVs," *Int. J. Control, Autom. Syst.*, vol. 12, no. 6, pp. 1266–1275, Dec. 2014.
[18] X.-H. Chang, Y. Liu, and M. Shen, "Resilient control design for lateral motion regulation of intelligent vehicle," *IEEE/ASME Trans. Mechatronics*, vol. 24, no. 6, pp. 2488–2497, Dec. 2019.
[19] X. Chang, J. H. Park, and J. Zhou, "Robust static output feedback H_∞ control design for linear systems with polytopic uncertainties," *Syst. Control Lett.*, vol. 85, pp. 23–32, Nov. 2015.
[20] C. Ren, R. Nie, and S. He, "Finite-time positiveness and distributed control of Lipschitz nonlinear multi-agent systems," *J. Franklin Inst.*, vol. 356, no. 15, pp. 8080–8092, Oct. 2019.
[21] C. Ren and S. He, "Finite-time stabilization for positive Markovian jumping neural networks," *Appl. Math. Comput.*, vol. 365, Jan. 2020, Art. no. 124631.
[22] C. Ren, S. He, X. Luan, F. Liu, and H. R. Karimi, "Finite-time L_2-gain asynchronous control for continuous-time positive hidden Markov jump systems via T–S fuzzy model approach," *IEEE Trans. Cybern.*, early access, Jun. 10, 2020, doi: 10.1109/TCYB.2020.2996743.
[23] H. Lee and H. J. Kim, "Estimation, control, and planning for autonomous aerial transportation," *IEEE Trans. Ind. Electron.*, vol. 64, no. 4, pp. 3369–3379, Apr. 2017.
[24] B. Yükesl, C. Secchi, H. H. Bülthoff, and A. Franchi, "A nonlinear force observer for quadrotors and application to physical interactive tasks," in *Proc. IEEE/ASME Int. Conf. Adv. Intell. Mechatronics*, Jul. 2014, pp. 433–440.
[25] M.-D. Hua, P. Morin, and C. Samson, "Balanced-force-control of underactuated thrust-propelled vehicles," in *Proc. 46th IEEE Conf. Decis. Control*, Dec. 2007, pp. 6435–6441.
[26] S. Kim, S. Choi, and H. J. Kim, "Aerial manipulation using a quadrotor with a two DOF robotic arm," in *Proc. IEEE Int. Conf. Intell. Robots Syst.*, Nov. 2013, pp. 4990–4995.
[27] V. Lippiello and F. Ruggiero, "Exploiting redundancy in Cartesian impedance control of UAVs equipped with a robotic arm," in *Proc. IEEE Int. Conf. Intell. Robots Syst.*, Oct. 2012, pp. 3768–3773.
[28] M. Kemper, "Control system for unmanned 4-rotor helicopter," European Patent 1 901 153, Mar. 19, 2008.
[29] S. Islam, P. X. Liu, A. E. Saddik, R. Ashour, J. Dias, and L. D. Seneviratne, "Artificial and virtual impedance interaction force reflection-based bilateral shared control for miniature unmanned aerial vehicle," *IEEE Trans. Ind. Electron.*, vol. 66, no. 1, pp. 329–337, Jan. 2019.
[30] D. Cho and H. J. Kim, "Fast adaptation for an uncertain nonlinear system using adaptive feedback linearization with optimal control modification," in *Proc. IEEE Conf. Decis. Control*, Dec. 2012, pp. 6083–6089.
[31] H. K. Khalil and J. Grizzle, *Nonlinear Systems*, Upper Saddle River, NJ, USA: Prentice-Hall, 2002.

YANJIE CHEN received the B.S. degree in electrical engineering and its automation from Southwest Jiaotong University, Chengdu, China, in 2011, and the M.S. and Ph.D. degrees in control science and engineering from Hunan University, Changsha, China, in 2013 and 2017, respectively. From 2014 to 2015, he was a Research Assistant with the Department of Engineering, National University of Singapore, Singapore. He is currently an Assistant Professor at the School of Mechanical Engineering and Automation, Fuzhou University, Fuzhou, China. His current research interests include robotics, motion planning, and artificial intelligence.

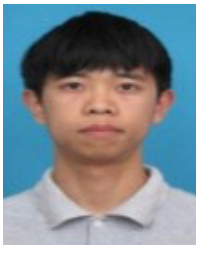

WEIWEI ZHAN received the B.S. degree from the Guilin University of Aerospace Technology, Guilin, China, in 2018. He is currently pursuing the M.S. degree with the School of Mechanical Engineering and Automation, Fuzhou University, Fuzhou, China. His research interests include aerial manipulator robot, control theory, and control engineering.

BINGWEI HE received the B.S. degree in mechanical engineering from Yanshan University, China, in 1996, and the M.S. and Ph.D. degrees in mechanical engineering from Xi'an Jiaotong University, in 1999 and 2003, respectively. He is currently a Professor at the School of Mechanical Engineering and Automation, Fuzhou University. His research interests include intelligent mechanical and medical engineering.

LIXIONG LIN received the B.S. degree in electrical engineering and automation from Huaqiao University, China, in 2008, the M.S. degree in detection technology from Xiamen University, China, in 2011, and the Ph.D. degree in control theory and control engineering from Xiamen University, in 2016. He is currently an Assistant Professor at the School of Mechanical Engineering and Automation, Fuzhou University. His research interests include fault detection, multi-sensor fusion, robotic control systems, and autonomous navigation.

ZHIQIANG MIAO (Member, IEEE) received the B.S. and Ph.D. degrees from the College of Electrical and Information Engineering, Hunan University, Changsha, China, in 2010 and 2016, respectively. From 2014 to 2015, he was a Visiting Scholar with The University of New Mexico, Albuquerque, NM, USA. From 2016 to 2018, he was a Postdoctoral Fellow with the Department of Mechanical and Automation Engineering, The Chinese University of Hong Kong, Hong Kong. He is currently an Associate Professor at the College of Electrical and Information Engineering, Hunan University. His current research interests include multi-robot systems, visual servoing, and nonlinear control.

XIAOFANG YUAN received the B.S., M.S., and Ph.D. degrees in electrical engineering from Hunan University, Changsha, China, in 2001, 2006, and 2008, respectively. He is currently a Professor at Hunan University. His research interests include intelligent control theory and application, industrial process control, and artificial neural networks.

YAONAN WANG received the B.S. degree in computer engineering from the East China University of Science and Technology, Fuzhou, China, in 1981, and the M.S. and Ph.D. degrees in control engineering from Hunan University, Changsha, China, in 1990 and 1994, respectively. He was a Postdoctoral Research Fellow with the National University of Defense Technology, Changsha, from 1994 to 1995, a Senior Humboldt Fellow in Germany, from 1998 to 2000, and a Visiting Professor with the University of Bremen, Bremen, Germany, from 2001 to 2004. He has been a Professor with Hunan University, since 1995. He has been a member of China Engineering Academy, since 2019. His current research interests include robot control, intelligent control and information processing, industrial process control, and image processing.